Effect of Model Formulation on Flow-Regime Predictions for Bubble Columns

Sarah M. Monahan and Rodney O. Fox
Dept. of Chemical and Biological Engineering, Iowa State Univ., 2114 Sweeney Hall, Ames, IA 50011

DOI 10.1002/aic.11042
Published online November 14, 2006 in Wiley InterScience (www.interscience.wiley.com).

It is well known that bubble-column flow-regime predictions of the Eulerian two-fluid model depend strongly on the model formulation. However, there is no general consensus on what force models must be included to match experiments for even the simplest flows. The flow simulated in this work corresponds to the bubble-column experiments of Harteveld with the additional assumptions of: (i) uniform-size (non-coalescing) bubbles, (ii) spatially uniform bubble injection, and (iii) non-deforming (spherical) bubbles. As in Monahan et al.'s 2005 article, the complete set of interphase force models includes drag, added-mass, lift, rotation, and strain. The simulation results are presented in the form of flow maps parameterized by the bubble Reynolds number and the average void fraction. As expected, the flow maps show a strong dependence on the model parameters; however, qualitatively only two types of flow maps are observed: (1) flows that transition from the homogeneous to the heterogeneous regime at relatively low average void fractions and (2) flows that transition at relatively high average void fractions (0.4–0.6) as are observed in the experiments. Remarkably, type-2 flow maps are only observed for two-fluid models that include the complete set of forces. © 2006 American Institute of Chemical Engineers *AIChE J,* 53: 9–18, 2007

Keywords: computational fluid dynamics, gas-liquid flow, buoyancy driven flow, two-fluid model, flow transitions, bubble columns, interphase force models

Introduction

The recent experiments of Harteveld[1] clearly demonstrate that homogeneous bubbly flow can be observed in carefully designed bubble-column experiments up to average void fractions exceeding 0.5. In stark contrast, Eulerian two-fluid models of homogeneous bubbly flow predict transition to non-uniform (such as rising continuity waves[2]) and heterogeneous flow (such as buoyant bubble plumes rising in a cooperative mode[3]) at significantly lower values of the average void fraction (usually much less than 0.2). This mismatch between theory and experiments would suggest that important force terms are missing in the two-fluid models currently used to model bubble columns. Indeed, in our previous work,[4] we demonstrated using numerical simulations that by adding new force terms representing "bubble-bubble" interactions,[5] the transition to heterogeneous flow could be suppressed up to much larger average void fractions. This intriguing observation motivated us to carry out the detailed investigation of the flow-regime predictions reported here.

In order to be consistent with the terminology used in experimental work, we shall refer to "homogeneous" bubbly flow as conditions under which the average void fraction is a (nearly) linear function of the inlet gas velocity. Note that this implies that a flow need not be "uniform" (that is, no spatial gradients) in order to be homogeneous. Following again the terminology used in experimental work, we will refer to "heterogeneous" flow as conditions under which the linear relation between av-

Correspondence concerning this article should be addressed to S. M. Monahan at monahan@iastate.edu.

erage void fraction and inlet gas velocity breaks down. In general, heterogeneous flows are observed in the simulations to correspond to "turbulent" bubbly flow, wherein large gradients in the local volume fraction lead to large-scale "chaotic" behavior. We shall make these terms more precise by showing examples of different flow behaviors later.

The intricate aeration system applied by Harteveld et al.[1,6,7] consisted of constant flow-rate air injection needles organized into groups in order to allow both uniform and non-uniform feed. The experiments were performed in simple column geometries (that is, round or rectangular cross sections) using well-defined aeration patterns, making them ideal choices for comparison with numerical simulations. Harteveld[1] demonstrated that the bubble size distribution created by the injection needles was very narrow, making it possible to assume in the simulations that all bubbles have the same diameter (approximately 4 mm). Also, due to their size and strong interactions with neighbors (at least at void fractions above 0.1–0.2), it is possible to approximate the bubble shape as a sphere in the simulations. At the high void fractions attained in the experiments, bubble coalescence could become an important factor, leading to rapid transition to heterogeneous flow. However, Harteveld[1] was able to suppress bubble coalescence by working with "aged" or "contaminated" water, since coalescence occurs more readily in pure liquids. In this manner, the flow transitions observed in the experiments were not caused by bubble coalescence, so the latter can be safely neglected in the simulations. Finally, as discussed by Mudde,[8] unlike in previous experimental studies that attempted to generate uniform inflow conditions (such as using porous plates), the Harteveld[1] experiments did not suffer from unanticipated disturbances that cause the gas inflow not to be truly uniform and time invariant. Thus, the uniform, time-invariant, constant-bubble-size inlet-flow boundary condition used in the simulations accurately represents the boundary conditions used in the Harteveld[1] experiments.

Many previous studies have focused on the prediction of flow-regime transitions using numerical simulations[9–11] or, more commonly, linear stability analysis of various model equations.[2,3,12–22] In general, two predominant instability modes have been identified: (1) a transition from uniform to non-uniform flow by way of rising plane waves (also called hindered rise[3]), and (2) a transition from uniform to heterogeneous flow by way of rising vertical bubble plumes (also called cooperative rise[3]). Note that the first instability mode can be observed in one-dimensional models that consider only the gradients in the vertical direction. In contrast, the second instability mode involves void-fraction disturbances in the horizontal direction, so that a two-dimensional model is required. We should also note that the first mode does not necessarily correspond to what is meant by "heterogeneous flow" in experimental studies. Indeed, as we shall see later, flows exhibiting rising plane waves can still show a linear dependence between the average void fraction and the inlet gas flow rate. This is not the case for rising bubble plumes where, due to cooperative rise, the "effective" bubble rise velocity is higher than for an isolated bubble, resulting in a lower average void fraction than would otherwise be observed at the same inlet gas flow rate. In the context of studying flow transitions using numerical simulations, these observations imply that at least a two-dimensional flow domain will be needed to capture the transition from homogeneous to heterogeneous flow.

Several relevant observations can be made concerning the previous theoretical work on flow transitions in bubble columns. First, one frequently finds statements such as "the transition occurs at void fractions in agreement with experiments." At face value, there is nothing extraordinary about such statements. However, on further reflection, one must ask, "which experiments?" (See Mudde[8] for a detailed discussion of problems associated with most experimental setups.) Indeed, from the experimental results presented in Harteveld[1] using various spargers (such as porous solid, perforated plates, needles, and so forth), different injection profiles, and considering even the "age" of the water, it is clear that the transition can occur over a very wide range of average void fractions. Thus, since the two-fluid models used in this and previous theoretical studies do not account for these parameter variations or for flow-generated disturbances in the inlet flow conditions, it is doubtful whether the comparison of a theoretical prediction with previous experiments would have any value for judging the quality of the model.

Second, nearly all of the theoretical studies implicitly assume that "homogeneous flow" seen in experiments corresponds to "uniform flow" in the model. Thus, when the uniform-flow solution in the model becomes linearly unstable, it is almost always taken to correspond to the transition to heterogeneous flow. At face value, this might also appear to be a reasonable assumption. However, as noted earlier, rising plane waves (which are very difficult to measure experimentally due to the inability to "look inside" the flow[1,23,24]) can also be considered "homogeneous" flow. Thus, it is difficult at best to judge the applicability of one-dimensional models to bubble-column flows, and the relative importance of the various modifications (such as accounting for bubble deformation or turbulent transport due to "large-scale" turbulent fluctuations) that have been suggested to bring them closer to experiments. On the other hand, the cooperative-rise instability found in two-dimensional models does lead to large-scale "turbulent" flow structures, and would be considered as leading to heterogeneous flow. Comparatively speaking, this instability has been investigated to a lesser extent (mainly in the context of the role of the lift force[3,21]), but it has been found that linear stability analysis predicts a transition to heterogeneous flow at average void fractions much lower than that observed by Harteveld,[1] assuming, of course that reasonable values are used for the model coefficients.

The deficiency of existing two-fluid models and the tendency towards "over fitting" the parameters to agree with a particular experiment has been noted by Mudde.[25] Another important point of disagreement noted by Mudde[8,25] is the relative instability of numerical models for uniformly sparged bubble columns to small perturbations. In their experiments at high void fractions, Harteveld et al.[6] found that the homogeneous flow regime is very stable to flow perturbations. In contrast, in our previous work,[4] we found that (except for a particular set of force models described below) the two-fluid model is very unstable and predicts transient "turbulent" flow in fully resolved, time-dependent, two- and three-dimensional simulations. In light of the predictions from linear stability analysis discussed above, this observation might not be surprising. However, at the very least, it does suggest that most two-fluid models presently used for modeling bubble columns are missing important physics.

To the best of our knowledge, the only two-fluid model that can predict homogeneous flow up to gas fractions of 0.5 is the one proposed by Kashiwa[5] that includes lift, rotation, and

strain forces. In the original derivation, these forces were expressed as attraction and repulsion, and took the form of a second-order tensor, constructed from the deformation rates of the velocity fields, multiplied by the velocity difference between the two phases. In our previous work,[4] we showed that an alternative representation of these attraction and repulsion forces is to express them in three parts: (i) lift, (ii) rotation, and (iii) strain. It should be noted that the lift force arising from the attraction/repulsion terms has the same form, but not the same origin, as the usual lift force involving a single bubble. More details on the force model are given below, but for the present discussion the important point is that without the lift, rotation, and strain forces, a homogeneous flow will transition to heterogeneous flow very quickly.[4] We are, thus, motivated to investigate the role of model formulation on flow transitions in greater detail using numerical simulations in order to determine the "minimal" model required for predicting stable homogenous flow at high void fractions.

The rest of this work is organized as follows. First, we provide a review of the two-fluid model formulation applied in our simulations. In the model formulation, the bubble Reynolds number (Re) is controlled by bubble diameter, and average void fraction ($\bar{\alpha}_d$) is controlled by the inlet gas flow rate. We present flow maps to identify the regions in Re-$\bar{\alpha}_d$ space where the flow profiles (such as void fraction contours) exhibit a particular behavior, and to clearly illustrate where flow transitions occur, and we show how these maps depend on the model formulation used. Additionally, we briefly examine the behavior of the force-model components at selected flow regimes. Finally, conclusions are drawn in the closing section of the article.

Description of the Two-Fluid Model

In this work, numerical studies are performed with CFDLib v. 99.2, a multiphase simulation library developed at Los Alamos National Laboratory, USDOE.[26] The code uses a cell-centered, finite-volume technique to integrate the time-dependent, multi-fluid equations of motion that govern multiphase flows. In this work, a Eulerian two-fluid model is employed to simulate incompressible, unsteady flow in bubble columns. The physical parameters correspond to air and water at room temperature and pressure. Mass transfer between the phases and bubble coalescence are not considered. Subscript c refers to the continuous (liquid) phase, and subscript d refers to the dispersed (bubble) phase. Additionally, α, ρ, and $\boldsymbol{u}$ correspond to volume fraction, density, and velocity, respectively.

The mass balance for phase k ($= c, d$) is expressed as:

$$\frac{\partial \alpha_k \rho_k}{\partial t} + \nabla \cdot (\alpha_k \rho_k \boldsymbol{u}_k) = 0. \tag{1}$$

The momentum balance for phase k is given by:

$$\alpha_k \rho_k \frac{\partial \boldsymbol{u}_k}{\partial t} + \alpha_k \rho_k \boldsymbol{u}_k \cdot \nabla \boldsymbol{u}_k = (-\alpha_k \nabla p - \nabla P_k) + \nabla \cdot \alpha_k \mu_{eff,k} \left[\nabla \boldsymbol{u}_k + (\nabla \boldsymbol{u}_k)^T \right] + \sum_f \boldsymbol{F}_{fk} + \alpha_k \rho_k \boldsymbol{g}. \tag{2}$$

The terms on the right-hand side of Eq. 2 represent, from left to right, the pressure gradient, bubble pressure, effective stress, interfacial momentum exchange, and the gravitational force. The closures for bubble pressure, effective stress, and interfacial momentum exchange are discussed next.

Bubble-pressure model

The bubble-pressure model represents the transport of momentum due to bubble-velocity fluctuations, collisions, and hydrodynamic interactions, and is assumed in the literature to play an important role in bubble-phase stability.[27] In this work, we apply the bubble-pressure model proposed by Biesheuvel and Gorissen[2]:

$$P_d = \rho_c C_{BP} \alpha_d |\boldsymbol{u}_d - \boldsymbol{u}_c|^2 H(\alpha_d), \tag{3}$$

where:[28]

$$H(\alpha_d) = \left(\frac{\alpha_d}{\alpha_{dcp}} \right) \left(1 - \frac{\alpha_d}{\alpha_{dcp}} \right). \tag{4}$$

In Eq. 3, C_{BP} is the added-mass coefficient of an isolated bubble, and α_{dcp} in Eq. 4 is the void fraction at close packing (set equal to 1.0 for our simulations). Note that in this work, the bubble-pressure term appears only in the momentum balance for the dispersed phase (that is, $P_c = 0$).

Effective viscosity

The stress term for phase k ($= c, d$) is expressed as:

$$\nabla \cdot \alpha_k \mu_{eff,k} \left[\nabla \boldsymbol{u}_k + (\nabla \boldsymbol{u}_k)^T \right], \tag{5}$$

where $\mu_{eff,k}$ represents the effective viscosity. In this work, the effective viscosity for the continuous phase is equal to the sum of the molecular viscosity of the continuous phase and a value for "turbulent viscosity": $\mu_{eff,c} = \mu_{0,c} + \mu_{t,c}$. Recall that in homogeneous flow, only so-called "pseudo-turbulence" and not large-scale turbulence is present, which differ by an order of magnitude in energy.[1] It would, thus, be inappropriate to model the turbulent viscosity in homogeneous flow by invoking a multiphase turbulence model such as the k-epsilon model. In our previous work,[4] the effective viscosity for the dispersed phase was equal to the molecular viscosity of the dispersed phase, or $\mu_{eff,d} = \mu_{0,d}$. Additional studies were subsequently performed to determine changes in flow behavior when the effective viscosity is used for both phases.[29] However, the changes in the flow transitions were found to be very small and will not be reported here. In this work, Sato's bubble-induced turbulence (BIT) model[30] is used to determine the pseudo-turbulent effective viscosity:

$$\mu_{t,c} = C_{BT} \rho_c d_b \alpha_d |\boldsymbol{u}_d - \boldsymbol{u}_c|. \tag{6}$$

The model constant C_{BT} is set equal to 0.6.[31] Note that at low bubble Reynolds numbers (small d_b), the BIT model has diminishing effect on the flow. However, our previous work[4] has shown that including a BIT model is essential for predicting homogeneous flow at higher bubble Reynolds numbers.

Interfacial momentum exchange

The interfacial momentum exchange describes the interaction between the continuous and dispersed phases. In CFDLib,

the total interfacial force acting on either of the phases can be expressed by the sum of the drag, added-mass, lift, rotation, and strain forces:

$$\sum_f \boldsymbol{F}_{fk} = \boldsymbol{F}_{D,k} + \boldsymbol{F}_{vm,k} + \boldsymbol{F}_{L,k} + \boldsymbol{F}_{rot,k} + \boldsymbol{F}_{S,k}. \quad (7)$$

It should be noted that Eq. 7 is presented and will be discussed as it would appear in the momentum balance for the dispersed phase (Eq. 2). The opposite sign is used when Eq. 7 is defined for the continuous phase.

The drag force is exerted on bubbles traveling steadily through a fluid, and is defined in CFDLib as:

$$\boldsymbol{F}_D = -\alpha_d \alpha_c \rho_c C_D(Re) \frac{3}{4 d_b} |\boldsymbol{u}_d - \boldsymbol{u}_c| (\boldsymbol{u}_d - \boldsymbol{u}_c), \quad (8)$$

where the bubble Reynolds number is defined by:

$$Re = \frac{d_b |\boldsymbol{u}_d - \boldsymbol{u}_c|}{v_c}. \quad (9)$$

For the drag coefficient, CFDLib uses the following relationship:[26]

$$C_D(Re) = C_\infty + \frac{24}{Re} + \frac{6}{1+\sqrt{Re}}. \quad (10)$$

where C_∞ has a nominal value of 0.5. We also tested another drag coefficient that is known to be appropriate for bubbly flow:[32]

$$C_D = max\left[\frac{24}{Re}(1 + 0.15 Re^{0.687}), \frac{8}{3}\frac{Eo}{(Eo+4)}\right], \quad (11)$$

where the Eötvös number is defined by:

$$Eo = \frac{g \rho_c d_b^2}{\sigma}. \quad (12)$$

However, we found that applying Eq. 11 resulted in qualitative predictions similar to those obtained when applying Eq. 10.[29] We can also note that the form of Eq. 8 corresponds to a Richardson-Zaki exponent of $n = 1$, and thus the drag force is neutral to both hindered ($n > 1$) and cooperative ($n < 1$) bubble rise.[3] The choice of $n = 1$ corresponds to the linear relation between the average void fraction (in the range of 0.06–0.25) and the inlet gas flow rate that is observed in the experiments.[7] Moreover, consistent with other studies,[10] our limited experience with using values for n other than unity has revealed that flow transitions occur at lower average void fractions (that is, the flow is less stable).

The added-mass force is defined in CFDLib as:

$$\boldsymbol{F}_{vm} = -\alpha_d \alpha_c \rho_v C_{vm} \left[\left(\frac{\partial \boldsymbol{u}_d}{\partial t} + \boldsymbol{u}_d \cdot \nabla \boldsymbol{u}_d\right) - \left(\frac{\partial \boldsymbol{u}_c}{\partial t} + \boldsymbol{u}_c \cdot \nabla \boldsymbol{u}_c\right)\right], \quad (13)$$

where ρ_v denotes the volume-averaged density, $\rho_v = \alpha_c \rho_c + \alpha_d \rho_d$. In this work, the added-mass coefficient C_{vm} is assumed to be 0.5. As shown by Minev et al.,[16] this form of the added-mass term leads to less stable uniform flows based on linear stability analysis. Nevertheless, we include it because of its importance in gas-liquid flows.

The remaining interfacial momentum exchange models are represented in CFDLib as the sum of attraction and repulsion forces, developed by Kashiwa:[5]

$$\boldsymbol{F}_{att} + \boldsymbol{F}_{rep} = \alpha_c \alpha_d \rho_v \boldsymbol{G} \cdot (\boldsymbol{u}_c - \boldsymbol{u}_d), \quad (14)$$

where the matrix $\boldsymbol{G}$ is equal to:[5]

$$\boldsymbol{G} = (C_{rep}/2)\left[(\nabla \boldsymbol{u}_c + \nabla \boldsymbol{u}_d) + (\nabla \boldsymbol{u}_c + \nabla \boldsymbol{u}_d)^T\right] - C_{att}\left[(\nabla \boldsymbol{u}_c + \nabla \boldsymbol{u}_d) - (\nabla \boldsymbol{u}_c + \nabla \boldsymbol{u}_d)^T\right]. \quad (15)$$

Note that $\boldsymbol{G}$ represents the sum of a symmetric tensor and an antisymmetric tensor. The symmetric tensor in $\boldsymbol{G}$ represents the sum of the rate-of-strain tensors for each phase. The antisymmetric part of $\boldsymbol{G}$ represents the sum of the vorticity tensors for each phase. The dot product of the antisymmetric tensor in $\boldsymbol{G}$ with $(\boldsymbol{u}_c - \boldsymbol{u}_d)$ can be expressed[29] as the sum of a lift force:

$$\boldsymbol{F}_L = \alpha_c \alpha_d \rho_v C_L (\boldsymbol{u}_d - \boldsymbol{u}_c) \times \nabla \times \boldsymbol{u}_c, \quad (16)$$

and a rotation force:

$$\boldsymbol{F}_{rot} = \alpha_c \alpha_d \rho_v C_{rot} (\boldsymbol{u}_d - \boldsymbol{u}_c) \times \nabla \times \boldsymbol{u}_d, \quad (17)$$

where $C_{att} = C_L = C_{rot}$.

Similarly, the dot product of the symmetric tensor in $\boldsymbol{G}$ with $(\boldsymbol{u}_c - \boldsymbol{u}_d)$ yields the strain force, with the strain coefficient C_S equal to $C_{rep}/2$:[29]

$$\boldsymbol{F}_S = \alpha_d \alpha_c \rho_v C_S \left[(\nabla \boldsymbol{u}_c + \nabla \boldsymbol{u}_d) + (\nabla \boldsymbol{u}_c + \nabla \boldsymbol{u}_d)^T\right] \cdot (\boldsymbol{u}_c - \boldsymbol{u}_d). \quad (18)$$

To the best of our knowledge, the attraction and repulsion terms (which are first-order in velocity gradients) developed by Kashiwa[5] have not appeared in two-fluid models previously discussed in the literature. However, we have observed that including these forces suppresses flow transitions[4] up to relatively large values for the average void fraction. Finally, it should be noted that in this study, we have limited ourselves to fixed values for the force coefficients and focused on the effect of turning off/on particular force terms.

Results and Discussion

Our previous work[4] showed that homogeneous and transitional flow behavior could be predicted in 6-cm columns with the BIT model and all force-model terms enabled with $C_L = C_{rot} = 0.375$ and $C_S = 0.125$. Additionally, we demonstrated that the bubble Reynolds number Re is controlled by bubble diameter, and average void fraction $\bar{\alpha}_d$ is controlled by inlet gas velocity u_g. Thus, we conjecture here that for given values of Re and $\bar{\alpha}_d$, the flow behavior will be the same for a particular set of force models. To test this conjecture, we have used numerical simulations to construct flow maps to find the regions in Re-$\bar{\alpha}_d$ space where the flow exhibits a particular behavior. As noted earlier, these numerical simulations are based on the experiments performed by Harteveld.[1,7] In these experiments,

Table 1. Inlet Gas Velocity and Average Void Fraction for Delft 2D Bubble Column

u_g (cm/s)	$\bar{\alpha}_d$ (Exp)
1.5	0.061
1.7	0.076
2.5	0.11
3.2	0.16
3.9	0.20
4.9	0.25

it was found that uniform aeration yields homogeneous flow for inlet gas velocity ranging from 1.5 cm/s to 4.9 cm/s (shown in Table 1), while, for example, having non-aerated sections near the column walls results in large-scale flow structures.[7]

It should be noted that we have adjusted C_∞ slightly[29] from the nominal value of 0.5 in order to predict the experimentally observed[7] average void fraction for a given value of the inlet gas velocity (Table 1). To assure that the CFDLib drag force model was adjusted properly, two simulations were considered: one at the lowest inlet-gas velocity used in the Delft experiments (1.5 cm/s), and one at the highest inlet-gas velocity (4.9 cm/s). Note that in these test cases, the input bubble diameter selected was approximately 4 mm, the average size observed by Harteveld.[1] Our simulations utilized a 2D domain of width 24.3 cm and height 48.6 cm (twice the column width), as noted in Table 2. For both phases, free-slip boundary conditions were applied at the vertical walls, gas velocity inflow was applied at the bottom of the column, and an outflow condition was applied at the top. As done in our previous work,[4] a grid-resolution study was carried out beforehand with uniform cell spacing as small as 0.1215 cm. A uniform cell spacing of 0.243 cm was found to yield grid-independent flow structures and was, therefore, used for all simulation results reported here. Table 3 shows the quantitative comparison between the simulation results and the Delft experimental data.[7] It can be seen in Table 3 that the simulations predicted slightly higher average void fractions than were observed in experiments (which is expected due to systematic experimental error, for example, a slight variation of bubble size with inlet flow rate[1]). The water volume-fraction profiles obtained for the simulations were homogeneous over the range of gas-flow rates used in these experiments (that is, average void fractions up to 0.25). Note also that the bubble rise velocity was independent of the inlet gas flow for both the experiments and the test-case simulations, which is consistent with using a Richardson-Zaki exponent of unity in the drag force (Eq. 8).

Flow maps

In order to cover the entire range where flow transitions occur, 42 simulations were performed with fixed values of the input bubble diameter d_b and the inlet gas flow rate. The target values considered for Re were 100, 400, 700, 1000, 1300, 1600, and 1900, corresponding to input values of $d_b \approx 1.19$, 2.78, 3.96, 4.98, 5.89, 6.74, and 7.54 mm, respectively. The target values considered for the average void fraction $\bar{\alpha}_d$ were 0.1, 0.2, 0.3, 0.4, 0.5, and 0.6. A description of the method used to determine the input value for d_b to yield the target Re and the input value of u_g to yield the target $\bar{\alpha}_d$ can be found in Monahan.[29] In general, the simulations returned the target values for Re and $\bar{\alpha}_d$, except when the flow transitioned to heterogeneous flow.

Table 2. Simulation Parameters

Column width	24.3 cm
Column height	48.6 cm
Number of cells in x-direction	100
Number of cells in y-direction	200
Grid cell spacing (square cells)	0.243 cm

The computational domain was the same as described previously. Each fully resolved, 2D, time-dependent simulation was run for a total of 15 sec in order to ensure that the flow statistics were independent of the initial conditions, and thus approximately 150 CPU hours on a 16-processor SunFire 6800 were needed for each of the 42 points on a flow map. Three force model cases were considered:

- Case (i): All forces enabled with $C_{vm} = 0.5$, $C_L = C_{rot} = 0.375$, and $C_S = 0.125$.
- Case (ii): Only drag force enabled.
- Case (iii): Drag and added-mass forces enabled.

Case (i) is the baseline model that includes all force terms used in our previous work for homogeneous flow.[4] Case (ii) is the "minimal" model that includes only drag (which cannot be neglected), and Case (iii) includes the added-mass term that is known to be important in gas-liquid flow.

Carrying out the simulations for the flow maps revealed that six different structure classifications were observed, as shown in Figure 1. In this figure, contour plots of the water volume fraction are plotted at the end of the simulation (15 sec). Because the amplitude of the fluctuations in the local void fraction depended on the flow regime, we have not used the same scaling in all plots. In general, the amplitude in the homogeneous regime was on the order of a few percent, while in the turbulent regime it was much larger. The profiles of swirls are characterized by small spatial inhomogeneities in the volume fraction. These structures tended to be no larger than 2 cm in width or length, and the change in local volume fraction with respect to position was gradual, not a steep gradient. It is important to also note that while the profiles of swirls or bands do not reflect uniform-flow behavior, the $\bar{\alpha}_d$ values that resulted from these profiles yielded a linear relationship between $\bar{\alpha}_d$ and u_g, which in experimental studies is taken as evidence of homogeneous flow. Only for transitional and turbulent flow profiles did the $\bar{\alpha}_d$ values deviate from linearity. It can also be seen in Figure 1 that the particular example of transitional flow shows both bands as well as more turbulent behavior. The reader can appreciate that the exact structure varied with time, and depended on the model formulation and Re.

Table 3. Void Fractions and Rise Velocity from Test-Case Simulations

	Case 1, $u_g = 1.5$ cm/s	Case 2, $u_g = 4.9$ cm/s
Average void fraction, simulation	0.0843	0.274
Average void fraction, experiments	0.061	0.25
Average rise velocity, simulation	17.79	17.77

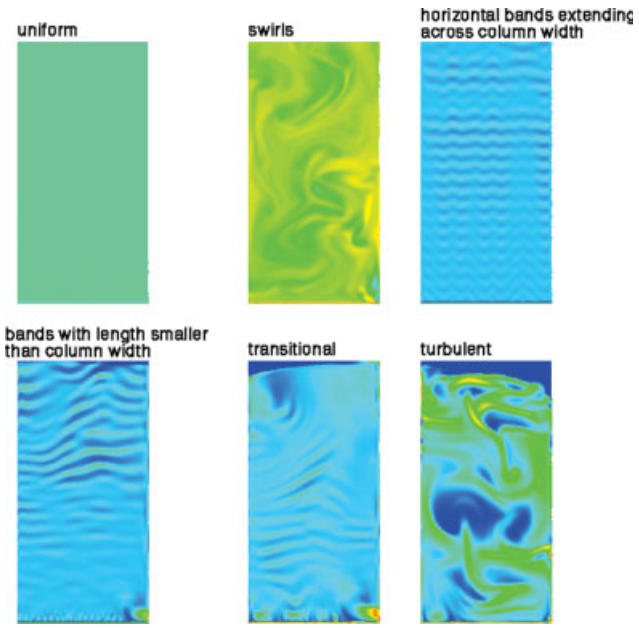

Figure 1. Continuous-phase volume-fraction profiles illustrating the representative flow structures observed in two-fluid simulations.

[Color figure can be viewed in the online issue, which is available at www.interscience.wiley.com.]

Figure 2 illustrates the flow map for Case (i), in which all force models were enabled. Note that the widest range of homogeneous flow was observed (without fitting any parameters except the drag model) for a bubble Reynolds number of 700. According to the flow map, when $Re \approx 700$, transition to turbulence occurred for $\bar{\alpha}_d$ near 0.5. This Re corresponds to approximately 4 mm bubbles in air-water systems, and this was the average bubble size observed in the Delft experiments.[1] Thus, the flow map agrees qualitatively with the Delft experiments for $Re \approx 700$, which showed that the flow was homogeneous for average void fractions up to 0.5. Additionally, the flow map reflects that Case (i) resulted in the greatest variation in possible flow structures, as the behavior progressed from uniform flow or swirls to horizontal bands to turbulence, with increasing Re and $\bar{\alpha}_d$. In general, for larger Reynolds numbers banded structures were observed, while for small Reynolds numbers transition to turbulent flow occurred directly from the uniform state. Note that, as shown in our previous work,[4] as the bubble Re decreases, the stabilizing effect of the BIT model is diminished. The BIT model (Eq. 6) is directly proportional to the bubble diameter, and thus has no effect at zero bubble diameter, or zero bubble Re. Additionally, for smaller values of Re (such as $< \sim 200$), the viscous term becomes less influential than the combined effect of the force models.[4] Thus, the transition to turbulent flow occurs earlier for smaller bubble-diameter bubbly flow. Note that the instability observed for very small bubbles may be an artifact of the well-known "ill-posed" nature of the inviscid two-fluid model,[33] and thus not be truly representative of real flows.

It may be noted that several simulations discussed in our previous work[4] also applied all force models and the BIT model. However, these simulations utilized the drag model with $C_\infty =$

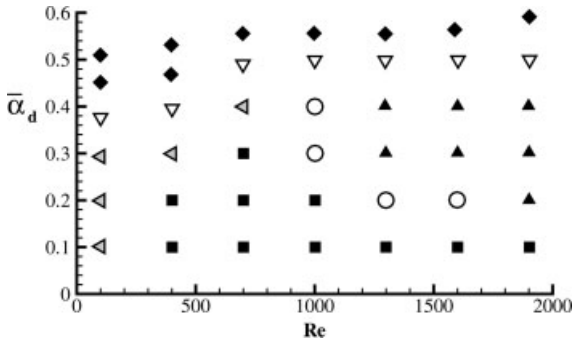

Figure 2. Flow map for Case (i).

Black squares: uniform flow; gray triangles: swirls; white circles: horizontal bands extending across column width; black triangles: horizontal bands with length smaller than column width; white triangles: transitional flow; black diamonds: turbulent flow.

0.5, and a uniform flow was obtained for $Re \approx 500$ and $\bar{\alpha}_d \approx 0.5$. This disagreement with the flow map presented in Figure 2 is due to the adjustment to the drag model[29] for the present study.

In experimental investigations of bubble columns, plots of the gas holdup versus the inlet gas velocity are often used to pinpoint the transition from homogeneous to heterogeneous flow.[9–11,18,19,34] Figure 3 shows the relationship between gas holdup and inlet gas velocity for Case (i). As seen in Figure 3, the value of $\bar{\alpha}_d$ falls below a straight line with respect to u_g at the transition to heterogeneous flow. In the (linear) homogenous regime, the slope of the line is a decreasing function of Reynolds number. In Figure 3, filled symbols along dotted lines correspond to $\bar{\alpha}_d$ obtained from simulations, while the open symbols along solid lines correspond to the linear relationship between $\bar{\alpha}_d$ and u_g that applies for homogeneous flow. As noted earlier, the banded structures did not deviate from this linear behavior. At the transition to turbulence the slope decreases continuously, indicating that the effective drag coefficient for the bubbles decreases in the turbulent regime.

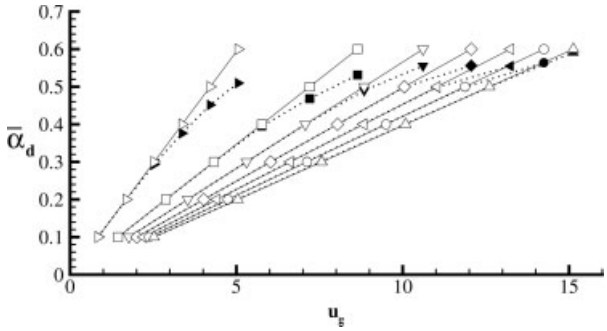

Figure 3. Average void fraction $\bar{\alpha}_d$ as a function of u_g for Case (i).

Filled symbols along dotted lines correspond to $\bar{\alpha}_d$ obtained from simulations, and open symbols along solid lines correspond to the linear relationship between $\bar{\alpha}_d$ and u_g that applies for homogeneous flow. Right-pointing triangles: $Re = 100$; squares: $Re = 400$; downward-pointing triangles: $Re = 700$; diamonds: $Re = 1000$; left-pointing triangles: $Re = 1300$; circles: $Re = 1600$; upward-pointing triangles: $Re = 1900$.

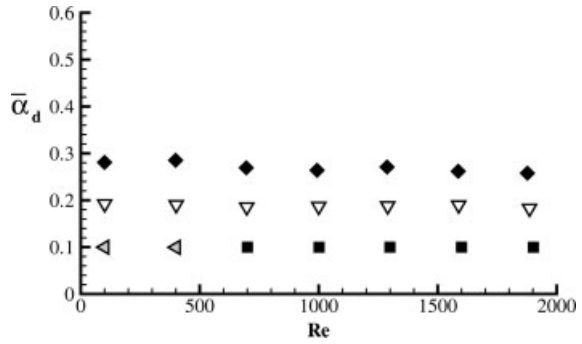

Figure 4. Flow map for Case (ii).

Black squares: uniform flow; gray triangles: swirls; white triangles: transitional flow; black diamonds: turbulent flow.

Note that unlike in many experiments where churn turbulence is observed,[10,11,18,19] the slope never becomes negative (nor is there a discontinuous jump to a lower line). We speculate that such behavior is due to bubble coalescence (which is not represented in our model), leading to an increase in the effective bubble diameter (and, hence, an increase in *Re* and a decrease in the drag coefficient).

In the literature on the two-fluid simulation of air-water bubble columns,[35] several researchers have concluded (often based on under-resolved simulations) that only the drag force is needed to adequately describe the fluid dynamics. Figure 4 illustrates the flow map for Case (ii), in which only the drag force was enabled. The map shows that the transition to the turbulent regime occurred for $\bar{\alpha}_d$ near 0.2 for all Reynolds numbers. Thus, using only the drag force is not in qualitative agreement with the Delft experiments,[1] which showed that homogeneous flow could be obtained for gas holdup values up to at least 0.5.

While drag is insufficient by itself to stabilize the flow, in bubbly flows the density of the continuous phase is large relative to the dispersed phase and it can be argued that the added-mass term cannot be neglected.[36] Figure 5 illustrates the flow map for Case (iii), in which only the drag and added-mass forces were enabled. According to this map, transition from homogeneous to turbulent flow occurred for $\bar{\alpha}_d$ approximately equal to 0.1–0.2. Both Cases (ii) and (iii) did not result in much variation of the possible flow structures observed, since the onset of turbulence occurred for smaller values of $\bar{\alpha}_d$ than observed for Case (i). Overall, the flow maps illustrate that the structures observed for a given value of *Re* and $\bar{\alpha}_d$ are highly dependent on the model parameters applied in the simulations, and that only Case (i) is in qualitative agreement with the Delft experiments.

Examination of force components

The flow maps and line plots presented in the previous section show that the force models have a significant effect on the transition regions observed. Thus, it is worthwhile to examine how selected force-model components behave for a particular model formulation. In this study, the average values of selected force-model components were determined for each of the horizontal planes in the column. We briefly examine the plane-averaged values of these force-model components as a function of column height for $Re = 1300$, $\bar{\alpha}_d \approx 0.1$ for Cases (i)–(iii).

Post-processing software was used to calculate all spatial derivatives from the simulation data in order to calculate the horizontal and vertical components of the drag, lift, rotation, and strain forces (Eqs. 8, 16, 17, and 18). It should be noted that for Cases (ii) and (iii), in which certain force models were disabled (that is, the force-model coefficient was set to zero in the simulation), spatial derivatives and, thus, the force-model components could still be calculated during post-processing. In other words, the force model may not have been included during the simulation, but the post-processing analysis allows us to calculate what the force-model components *would have been* for a given set of data obtained during the simulation. Subsequently, we can show how the force components *would have behaved* for each type of flow at approximately the same *Re* and $\bar{\alpha}_d$.

Finally, two scaling issues are addressed. First, the expression for the drag force in the uniform-flow state,

$$\boldsymbol{F}_{D0} = -\bar{\alpha}_d(1-\bar{\alpha}_d)\rho_c \frac{3}{4d_b} u_d(u_d \boldsymbol{i}) C_D, \tag{19}$$

was subtracted from the vertical component of the drag force defined in Eq. 8, resulting in $\boldsymbol{F}_{Dy,net} = \boldsymbol{F}_{Dy} - \boldsymbol{F}_{D0}$. In uniform flow, we would thus expect $\boldsymbol{F}_{Dy,net}$ to be null. Considering only the net vertical drag force component allows for an examination of the effect of drag on an order of magnitude more comparable to those of the other force-model components. Second, if the uniform rise velocity u_d is considered the characteristic velocity, the bubble diameter d_b is considered the characteristic length, and the continuous phase density ρ_c is considered the characteristic density, the force components can be made dimensionless by dividing by $(\rho_c u_d^2/d_b)$. All the force components discussed below have been made dimensionless in this manner.

We examine how the force-model components behaved for Cases (i)–(iii) with $Re = 1300$ and $\bar{\alpha}_d \approx 0.1$. For Case (i), homogeneous flow was observed. As the column height increased, the plane-averaged values of all the force-model components remained approximately zero (within the accuracy of the code). Any variations observed were on the order of 10^{-5} to 10^{-4} for the net drag force, and on the order of 10^{-6} for the lift, rotation, and strain forces. Such behavior corresponds to the uniform flow observed for $Re = 1300$ and $\bar{\alpha}_d \approx 0.1$.

Figure 6 shows how the force-model components behaved for Case (ii) with $Re = 1300$ and $\bar{\alpha}_d \approx 0.1$, when uniform flow was also observed. The net vertical drag component, $\boldsymbol{F}_{Dy,net}$, was approximately zero along the column height, as expected.

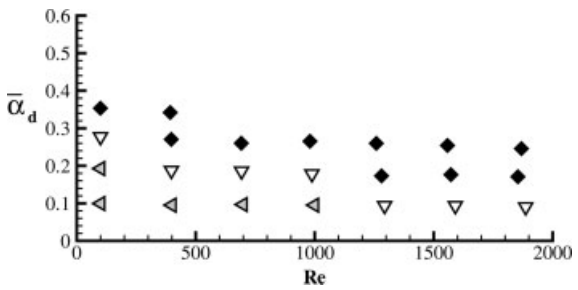

Figure 5. Flow map for Case (iii).

Gray triangles: swirls; white triangles: transitional flow; black diamonds: turbulent flow.

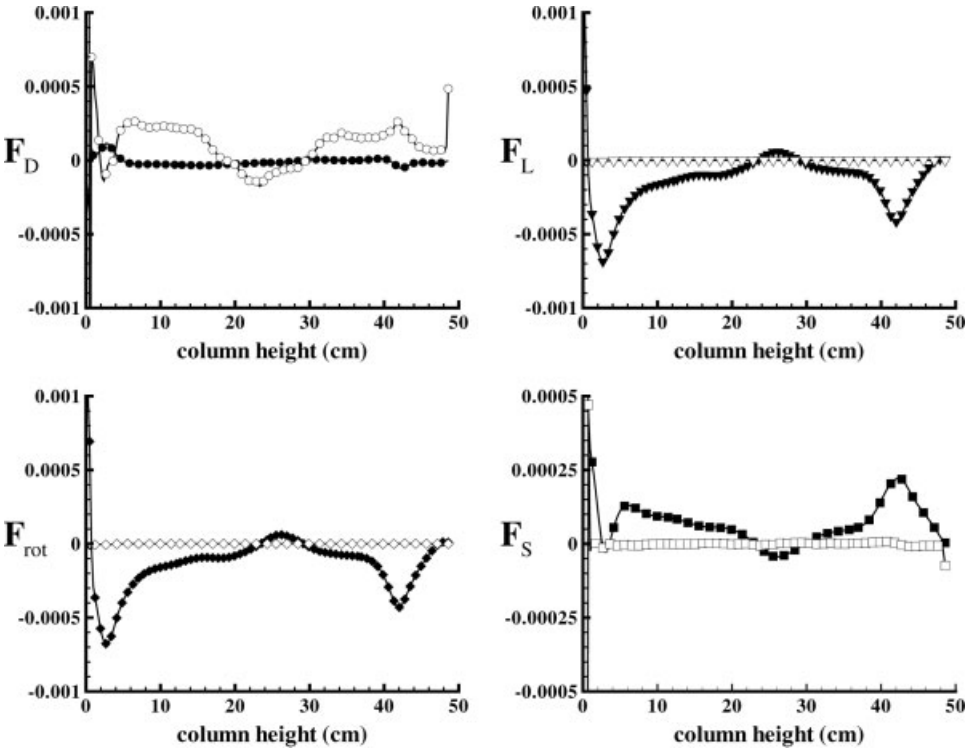

Figure 6. Force components for Case (ii) with $Re = 1300$ and $\bar{\alpha}_d = 0.1$.

Uniform flow is observed. Filled symbols represent horizontal force components, and open symbols represent vertical force components. Upper left: drag. Upper right: lift. Lower left: rotation. Lower right: strain.

Note that in the expression $\boldsymbol{F}_{Dy,net} = \boldsymbol{F}_{Dy} - \boldsymbol{F}_{D0}$, both $\boldsymbol{F}_{Dy}$ and $\boldsymbol{F}_{D0}$ are negative. Thus, when $\boldsymbol{F}_{Dy,net}$ is positive, it corresponds to $\boldsymbol{F}_{D0}$ having a greater influence than $\boldsymbol{F}_{Dy}$ (that is, $\boldsymbol{F}_{D0}$ is more negative than $\boldsymbol{F}_{Dy}$) on average for a particular plane, resulting in a larger rise velocity than in the uniform case. The lift and rotation components were relatively small along the column height. The plane-averaged vertical component of the strain force also remained small as column height increased, while the horizontal component varied weakly along the column height. As seen for Case (i), any variations among the plane-averaged force components were small ($\sim 10^{-4}$), corresponding to the expected uniform profile designated by the flow map for Case (ii) (Figure 4).

For Case (iii) with $Re = 1300$ and $\bar{\alpha}_d \approx 0.1$, transitional behavior was expected. Figure 7 shows that the plane-averaged components of all the forces varied significantly with increasing column height. The maximum absolute values observed were $\sim 10^{-2}$ for the net drag force, $\sim 5 \times 10^{-3}$ for the lift and rotation forces, and $\sim 2.5 \times 10^{-3}$ for the strain terms. The higher degree of variation observed for all the components corresponds to flow transitioning from uniform behavior. Additionally, note that $\boldsymbol{F}_{Dy,net}$ was positive throughout much of the column. This corresponds to $\boldsymbol{F}_{D0}$ having a greater influence than $\boldsymbol{F}_{Dy}$ (that is, $\boldsymbol{F}_{D0}$ is more negative than $\boldsymbol{F}_{Dy}$) on average for most of the planes considered within the column. As discussed previously, the effective drag coefficient in $\boldsymbol{F}_{Dy}$ for the bubbles is decreasing upon transition from uniform flow; and, thus, an increase in rise velocity $|\boldsymbol{u}_d - \boldsymbol{u}_c|$ occurs, which corresponds to the smaller $\bar{\alpha}_d$ value for which transitional or turbulent behavior was observed.

Finally, we should note that in all of our simulations, the lift-force coefficient (when used) was positive. Based on an analysis of the role of the lift force by Lucas et al.,[21] Harteveld[1] has speculated that the instability observed in his experiments was due to a change in sign of the lift force near the walls at the top of the bubble column. The transition from homogeneous to turbulent flow in Case (i) of our simulations cannot be attributed to a change in the sign of the lift force because the lift coefficient was held constant. Furthermore, because free-slip boundary conditions were used at the walls, the instability in Case (i) did not begin at the column walls, although it did originate near the top of the column. We, therefore, cannot directly check the influence of the velocity profile near the walls from our simulations. We can, however, conclude that all of the force terms, combined with a bubble-induced turbulence model, must be included in order to observe homogeneous flow up to high average void fractions. Indeed, if any one of these components is turned off, the transition to turbulent flow occurs at significantly lower values of the average void fraction. Unfortunately, when all forces are present, the transition to turbulent flow begins from a non-uniform (albeit homogeneous) state, which makes analytical studies (such as linear stability analysis) very difficult. We can speculate, however, that the role of the lift, rotation, and strain terms is to suppress the production of vorticity, and thus they counteract the vorticity production due to density gradients (that is, buoyancy-driven turbulence[37]). In any case, further study of the exact nature of the transition to turbulent flow and the role of the various force terms is needed in order to completely understand the controlling physical mechanisms in bubble columns.

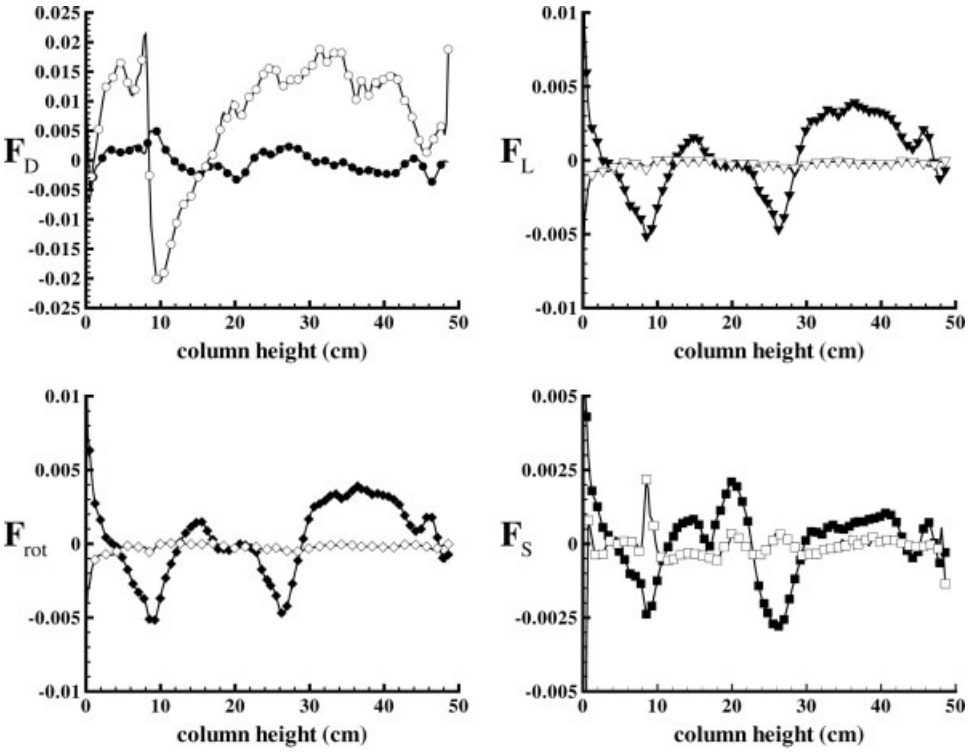

Figure 7. Force components for Case (iii) with $Re = 1300$ and $\bar{\alpha}_d \approx 0.1$.

Transitional behavior is observed. Filled symbols represent horizontal force components, and open symbols represent vertical force components. Upper left: drag. Upper right: lift. Lower left: rotation. Lower right: strain.

Conclusions

The overall conclusion from this study is that flow-regime predictions for bubble-column simulations must include the full set of force models in order to predict homogeneous flow at high average void fractions as observed in the experiments of Harteveld.[1] Applying all the force models results in homogeneous flow in the same range of inlet flow rates as those used in the Delft experiments.[6,7] Simulations over a wide range of bubble diameters and inlet gas flow rates were carried out in order to construct flow maps of the regions in Re-$\bar{\alpha}_d$ space where flow transitions occur. Using drag only or drag and added-mass, we illustrated the strong dependence of the predicted flow maps on the two-fluid model formulation. Visual observation of the flow transition suggests that large-scale structures originate near the top of the flow domain and eventually propagate through the entire bubble column, which is consistent with the experimental observations of Harteveld.[1] However, further work is needed to understand the effect of inhomogeneous velocity and void fraction profiles near the column walls, and the effect of the choice of boundary conditions used in the two-fluid model.

Acknowledgments

We are grateful to the National Science Foundation (CTS-0112571) for funding this work. Dr. Wouter Harteveld of Delft University has generously shared his experimental data with us and offered suggestions to consider in our numerical studies. Additionally, we would like to thank Dr. Kashiwa at Los Alamos National Laboratory for his assistance with CFDLib.

Notation

C_{att} = attraction coefficient
C_{BP} = added-mass coefficient of an isolated bubble
C_{BT} = proportionality constant for bubble-induced turbulence model
C_D = drag coefficient
C_L = lift coefficient
C_{rep} = repulsion coefficient
C_{rot} = rotation coefficient
C_S = strain coefficient
C_{vm} = added-mass coefficient
C_∞ = adjustable term within drag coefficient C_D (Re) in Eq. 10
d_b = bubble diameter, mm
Eo = Eötvös number, dimensionless
$\boldsymbol{F}_{att}$ = attraction force
$\boldsymbol{F}_D$ = drag force
$\boldsymbol{F}_{fk}$ = sum of interaction forces for momentum balance (either phase)
$\boldsymbol{F}_L$ = lift force
$\boldsymbol{F}_{rep}$ = repulsion force
$\boldsymbol{F}_{rot}$ = rotation force
$\boldsymbol{F}_S$ = strain force
$\boldsymbol{F}_{vm}$ = added-mass force
$\boldsymbol{g}$ = gravitational force
$\boldsymbol{i}$ = unit vector in the upward vertical direction
P_d = bubble-pressure model applied to dispersed phase
p = pressure
Re = bubble Reynolds number, dimensionless
$\boldsymbol{u}_c$ = velocity of continuous phase, cm/s
$\boldsymbol{u}_d$ = velocity of dispersed phase, cm/s
u_d = uniform rise velocity, cm/s
u_g = superficial gas velocity, cm/s

Greek letters

α_c = volume fraction of continuous phase, dimensionless
α_d = volume fraction of dispersed phase, dimensionless

$\bar{\alpha}_d$ = average void fraction, dimensionless
α_{dcp} = dispersed-phase void fraction at close packing, dimensionless
$\mu_{0,c}$ = molecular viscosity of continuous phase
$\mu_{0,d}$ = molecular viscosity of dispersed phase
$\mu_{eff,c}$ = effective viscosity of continuous phase
$\mu_{eff,d}$ = effective viscosity of dispersed phase
$\mu_{t,c}$ = pseudo-turbulent viscosity for continuous phase
v_c = kinematic molecular viscosity for continuous phase
ρ_c = density of continuous phase
ρ_d = density of dispersed phase
ρ_v = volume-averaged density
σ = surface tension, 72.8 dyne/cm

Subscripts

c = continuous phase
d = dispersed phase
f = index for sum of interfacial forces
k = general phase

Literature Cited

1. Harteveld W. *Bubble Columns: Structures or Stability?*, Ph.D. dissertation, Delft Univ. of Technology, the Netherlands; 2005.
2. Biesheuvel A, Gorissen WCM. Void fraction disturbances in a uniform bubbly fluid. *Int J Multiphase Flow*. 1990;16(2):211–231.
3. Sankaranarayanan K, Sundaresan S. Lift force in bubbly suspensions. *Chem Eng Sci*. 2002;57:3521–3542.
4. Monahan S, Vitankar VS, Fox RO. CFD predictions for flow-regime transitions in bubble columns. *AIChE J*. 2005;51:1897–1923.
5. Kashiwa B. On the Euler equations for multiphase flow. LA-UR-98831. Inst. for Multiphase Science and Technology 1998 Annual Meeting, Univ. of Santa Barbara, February 26–28, 1998.
6. Harteveld WK, Mudde RF, van den Akker HEA. Dynamics of a bubble column: influence of gas distribution on coherent structures. *Can J Chem Eng*. 2003;81(3–4):389–394.
7. Harteveld WK, Julia JE, Mudde RF, van den Akker HEA. Large scale vortical structures in bubble columns for gas fractions in the range 5%–25%. Proc of the 16th Int Conf on Chemical and Process Engineering, Prague, Czech Republic, 2004.
8. Mudde RF. Gravity-driven bubbly flows. *Ann Rev Fluid Mech*. 2005; 37:393–423.
9. Olmos E, Gentric C, Vial Ch, Wild G, Midoux N. Numerical simulation of multiphase flow in bubble column reactors. Influence of bubble coalescence and break-up. *Chem Eng Sci*. 2001;56:6359–6365.
10. Olmos E, Gentric C, Midoux N. Numerical description of flow regime transitions in bubble column reactors by a multiple gas phase model. *Chem Eng Sci*. 2003;58:2113–2121.
11. Olmos E, Gentric C, Poncin S, Midoux N. Description of flow regime transitions in bubble columns via laser Doppler anemometry signals processing. *Chem Eng Sci*. 2003;58:1731–1742.
12. Pauchon C, Banerjee S. Interphase momentum interaction effects in the averaged multifield model. Part I: Void propagation in bubbly flows. *Int J Multiphase Flow*. 1986;12(4):559–573.
13. Pauchon C, Banerjee S. Interphase momentum interaction effects in the averaged multifield model. Part II: Kinematic waves and interfacial drag in bubbly flows. *Int J Multiphase Flow*. 1988;14(3):253–264.
14. Van Wijngaarden L, Kapteyn C. Concentration waves in dilute bubble/liquid mixtures. *J Fluid Mech*. 1990;212:111–137.
15. Shnip AI, Kolhatkar RV, Swamy D, Joshi JB. Criteria for the transition from the homogeneous to the heterogeneous regime in two-dimensional bubble column reactors. *Int J Multiphase Flow*. 1992; 18(5):705–726.
16. Minev PD, Lange U, Nandakumar K. A comparative study of two-phase flow models relevant to bubble column dynamics. *J Fluid Mech*. 1999;394:73–96.
17. León-Becerril E, Liné A. Stability analysis of a bubble column. *Chem Eng Sci*. 2001;56(21–22):6135–6141.
18. Ruzicka MC, Zahradnik J, Drahos J, Thomas NH. Homogeneous-heterogeneous regime transition in bubble columns. *Chem Eng Sci*. 2001;56:4609–4626.
19. Ruzicka MC, Drahoš J, Fialová M, Thomas NH. Effect of bubble column dimensions on flow regime transition. *Chem Eng Sci*. 2001; 56:6117–6124.
20. Thorat BN, Joshi JB. Regime transition in bubble columns: experimental and predictions. *Exp Thermal Fluid Sci*. 2004;28:423–430.
21. Lucas D, Prasser H-M, Manera A. Influence of the lift force on the stability of a bubble column. *Chem Eng Sci*. 2005;60:3609–3619.
22. Bhole MR, Joshi JB. Stability analysis of bubble columns: predictions for regime transition. *Chem Eng Sci*. 2005;60:4493–4507.
23. Zenit R, Koch DL, Sangani AS. Measurements of the average properties of a suspension of bubbles rising in a vertical channel. *J Fluid Mech*. 2001;429:307–342.
24. Figueroza-Espinoza B, Zenit R. Clustering in high Re monodispersed bubbly flows. *Physics of Fluids*. 2005;17:091701.
25. Mudde RF. Towards modeling and simulations of industrial bubbly flows. Proc of the 11th Workshop on Two-Phase Flow Predictions, Merseburg, Germany, April 5–8, 2005.
26. Kashiwa BA, Padial NT, Rauenzahn RM, VanderHeyden WB. A cell-centered ICE method for multiphase flow simulations. ASME Symposium on Numerical Methods for Multiphase Flows, Lake Tahoe, Nevada, June 19–23, 1994. (LA-UR-93-3922.)
27. Spelt PDM, Sangani A. Properties and averaged equations for flows of bubbly liquids. *Appl Sci Res*. 1998;58:337–386.
28. Batchelor GK. A new theory on the instability of a uniform fluidized bed. *J Fluid Mech*. 1988;193:75–110.
29. Monahan S. *Computational Fluid Dynamics Analysis of Air-Water Bubble Columns*, Ph.D. dissertation, Iowa State Univ., IA, 2006.
30. Sato Y, Sekoguchi K. Liquid velocity distribution in two-phase bubble flow. *Int J Multiphase Flow*. 1975;2(1):79–95.
31. Sato Y, Sadatomi M, Sekoguchi K. Momentum and heat transfer in two-phase bubble flow I. *Int J Multiphase Flow*. 1981;7(2):167–177.
32. Tomiyama A, Kataoka I, Sakaguchi T. Drag coefficients of bubbles (1st report, drag coefficients of a single bubble in a stagnant liquid). *Nippon Kikai Gakkai Ronbunshu B Hen*. 1995;61(587):2357–2364.
33. Drew DA, Passman DL. *Theory of Multicomponent Fluids*. New York: Springer-Verlag; 1999.
34. Zahradnik J, Fialová M, Ruzicka M, Drahoš J, Kaštánek F, Thomas NH. Duality of the gas-liquid flow regimes in bubble column reactors. *Chem Eng Sci*. 1997;52:3811–3826.
35. Sokolichin A, Eigenberger G, Lapin A. Simulation of buoyancy driven bubbly flow: established simplifications and open questions. *AIChE J*. 2004;50(1):24–45.
36. Delnoij E, Lammers FA, Kuipers JAM, van Swaaij WPM. Dynamic simulation of dispersed gas-liquid two-phase flow using a discrete bubble model. *Chem Eng Sci*. 1997;52(9):1429–1458.
37. Ruzicka MC, Thomas NH. Buoyancy-driven instability of bubbly layers: analogy with thermal convection. *Int J Multiphase Flow*. 2003;29:249–270.

Manuscript received Dec. 14, 2005, revision received Jun. 29, 2006, and final revision received Oct. 9, 2006.